Directional Evaluation of Receive Power, Rician K-factor and RMS Delay Spread obtained from Power Measurements of 60 GHz Indoor Channels

E. Zöchmann[†*] M. Lerch[†] S. Caban[†] R. Langwieser[†]
C.F. Mecklenbräuker[†] M. Rupp[†]

***Abstract* — To meet link budgets for millimetre wave wireless communications, antennas with high directivity are essential. This directional view of the channel is evaluated by the important small scale fading parameters receive power, Rician K-factor and the RMS delay spread. These parameters are all derived from frequency swept power measurements. The effect of transmit polarization is very visual in the measurement results. A maximum K-factor of almost 80 was observed. The RMS delay spread is approximately 4 ns at reflective reception.**

1 INTRODUCTION

Millimetre wave signal processing algorithms [1] heavily rely on sparsity in the angular domain, that is, only a few dominant directions are impinging on the receive array. Previous works are mostly focusing on site-specific (azimuthal) angular power profile measurements [2–8] without evaluation on a sphere [9]. Further, the Rician K-factor and the RMS delay spread have been given too little attention.

Our receive power measurements do not reject the 3D sparsity assumption. As we carry out directional measurements of static channels, we use ergodicity and derive the K-factor from the transfer function as proposed in [10]. The RMS delay spread τ_{RMS} is estimated using the frequency domain level crossing rate L_f [11]. Analogous to the relation of mobile speed and time domain level crossing rate, there is a direct proportional relationship between L_f and τ_{RMS}. This method is very suitable for static indoor scenarios and continuous wave frequency sweeping methods.

2 MEASUREMENT SETUP

The transmitter (TX) is mounted in a corner of our laboratory at 2 m height, see Figures 1 and 2.

Figure 1: View from the transmitter to the receiver.

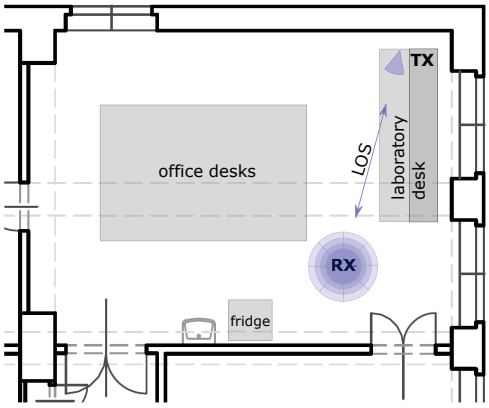

Figure 2: Floorplan of the measured environment.

The receive antenna, a conical 20 dBi horn, is mounted on a multi-axis positioning and rotating system, see Figure 3. The azimuthal and elevation angle are controlled to scan the whole upper hemisphere. The multi-axis system moves and rotates the horn antenna such that its front stays at the same x, y coordinate during the whole measurement.

2.1 Millimetre Wave Signal Generation and Reception

For millimetre wave signal generation and reception, we use Pasternack modules[1] that serve as up

*Christian Doppler Laboratory for Dependable Wireless Connectivity for the Society in Motion, TU Wien, Austria ezoechma@nt.tuwien.ac.at
[†]Institute of Telecommunications, TU Wien, Austria

[1]The modules are based on RFICs described in [12].

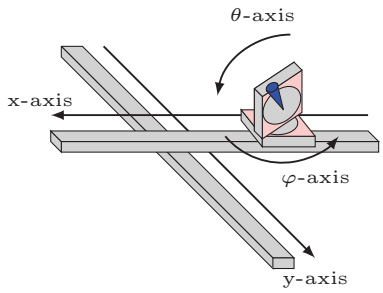

Figure 3: Drawing of the mechanical setup used for directional scanning.

and down-converter from baseband to V-band, see Figure 4. These modules are operating built-in synthesizer PLLs. Within these PLLs, the reference frequency of 278.514 MHz is more than 20 fold multiplied, leading to strong phase noise.

2.2 Transfer Function Measurement

We use an R&S ZVA24 vector network analyser to measure the forward transfer function S_{21}. To avoid crosstalk, we operate the transmitter and receiver at different baseband frequencies: 601 to 1100 MHz and 101 to 600 MHz. To suppress the mirror frequencies, the LO at the receiver is 500 MHz higher than the LO at the transmitter, see Figure 4. Due to the strong phase noise, we only measure the magnitude of the S_{21} parameter and disregard the phases.

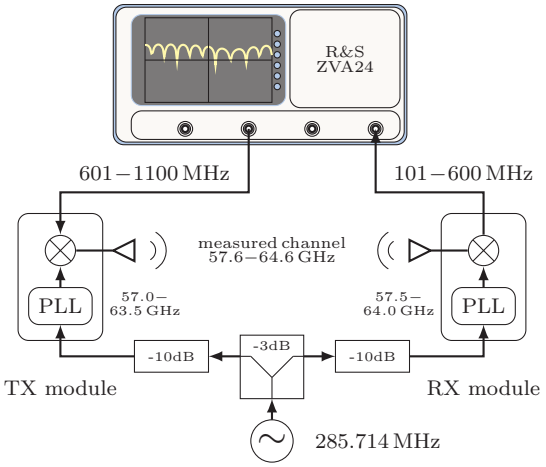

Figure 4: Transfer function measurement setup using the conversion gain (mixer) measurement option of the R&S VNA.

2.3 Dynamic Range of the Results

The sensitivity of the VNA is roughly −70 dBm. The output port power of the VNA is set to −30 dBm. The maximum receive power is obtained for a LOS connection. For 5 m distance, we calculate a free space path loss of approximately 82 dB. The amplification of the transmitter and receiver sums up to 60 dB, so that the maximum input level at the VNA with 20 dBi horn antennas at both sites equals −12 dBm. The dynamic range of the power measurement is therefore bounded by 58 dB. Our receiver is not shielded, which limits the directivity by spurious emissions from the PCB. The large dynamic range is therefore not visual in the results.

The largest Rician K-factor that can be realised by our setup was tested via back-to-back calibration. Theoretically, the K-factor of the calibrated direct connection of TX and RX through an attenuator should tend to infinity. We measured a K-factor of far above thousand.

Since noise leads to additional level crossings, the RMS delay spread retrieved from L_f is generally too high, especially for weaker signals. This is analysed in detail in [13].

3 PARAMETER ESTIMATION

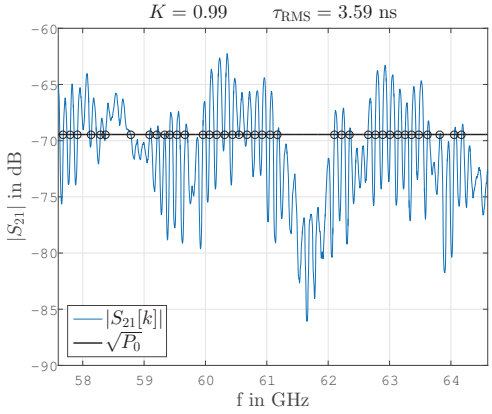

Figure 5: Examplary channel trace showing level crossings through the RMS amplitude.

After the receive antenna was rotated to a specific azimuth and elevation angle, $|S_{21}|$ is measured and corrected by back-to-back calibration data. Having $|S_{21}|$ at hand, the steps below are used to extract all parameters of interest [11]:

Firstly, the relative receive power is estimated as $P_0 = {}^1/_{N_K} \sum_{k=1}^{N_K} |S_{21}[k]|^2$, where $k = 1, \ldots, N_K$ are the measured frequency indices. The RMS amplitude is $\sqrt{P_0}$.

Secondly, the Rician K-factor is estimated from the moment relation [10] ${}^1/\sqrt{P_0} N_K \sum_{k=1}^{N_K} |S_{21}[k]| \approx {}^{\mathbb{E}\{|S_{21}[k]|\}}/\sqrt{\mathbb{E}\{|S_{21}[k]|^2\}} = \sqrt{\frac{\pi}{4(K+1)}} e^{-K/2} \left[(K+1) I_0\left({}^K/_2\right) + K I_1\left({}^K/_2\right)\right]$, where $I_n(\cdot)$ denotes the modified Bessel function of first kind n^{th} order.

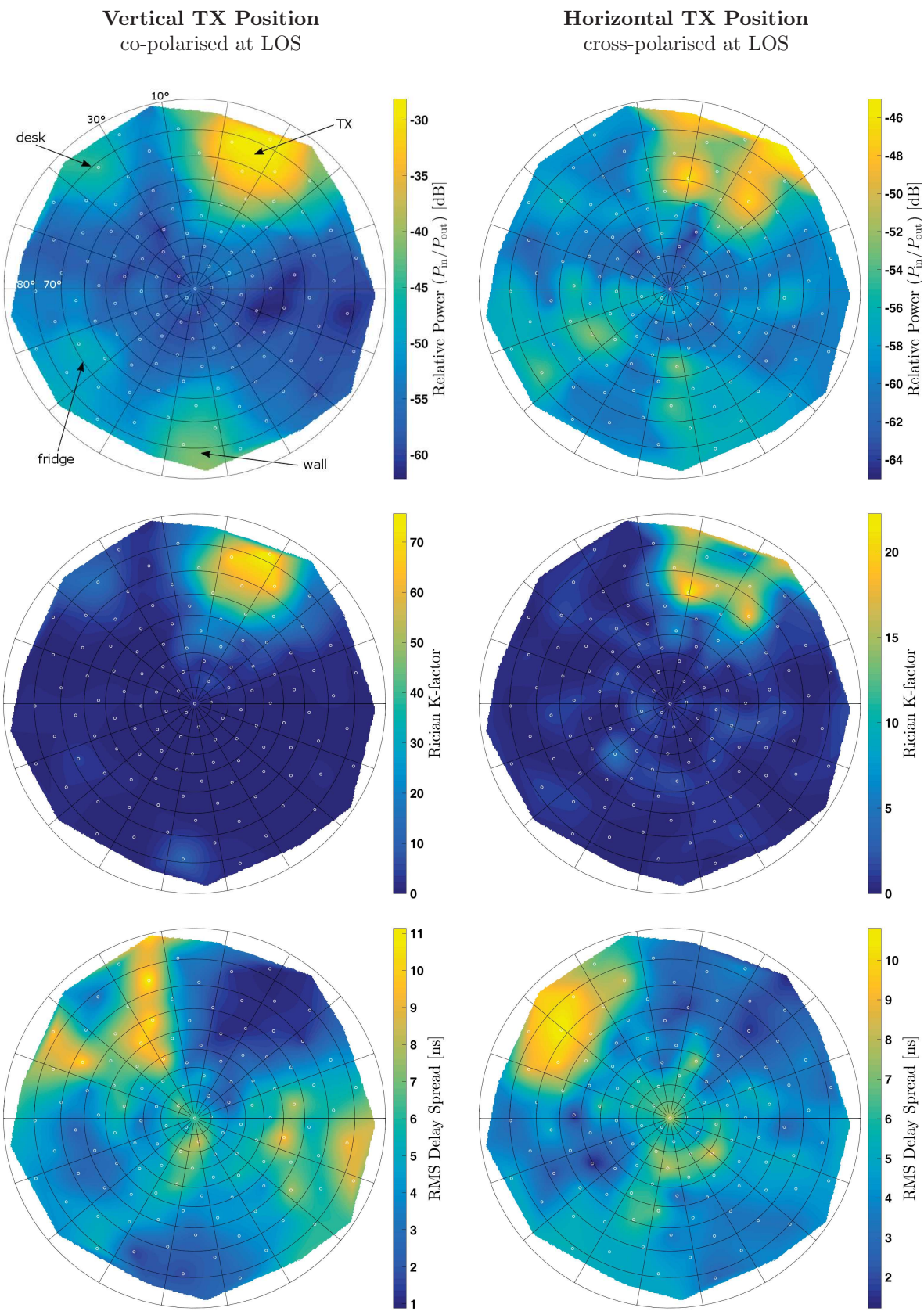

Figure 6: Relative receive power (input power at VNA relative to output power), Rician K-factor and RMS delay spread for both transmit polarisations. The left column shows measurement results, where the LOS connection has aligned polarization (co-pol) and the right column shows the scenario, where the transmit and receive antenna polarisation is perpenticular at LOS. The black concentric circles are latitudes and the black array of lines show longitudes. The white indicators '○' show the measurement positions.

Thirdly, the relation $L_f = \tau_{\mathrm{RMS}} f(\sqrt{P_0}, K)$ is used to find τ_{RMS}. The proportionality function $f(\cdot)$ can be found in [11]. The level crossing rate L_f was determined at the RMS amplitude $\sqrt{P_0}$, see Figure 5 for an exemplary channel trace.

We spent 201 frequency points per 500 MHz fraction which gives a frequency spacing f_s close to the sampling theorem's limit $\frac{1}{f_s} \geq 2\,\tau_{\mathrm{MAX}} = 2 \cdot 200\,\mathrm{ns}$, to collect as little noise as possible [13]; τ_{MAX} is three times higher than previously reported results [14].

4 MEASUREMENT RESULTS

The transmitter is turned 90° for two different polarisations at the LOS connection. We see a similar polarization behaviour as demonstrated in [7].

Through spiral sampling on a sphere, the sampling points are spaced equidistantly. The results are visualised via the stereographic projection from the south pole, see Figure 6. We used $\tan(\theta/2)$ as azimuthal projection.

Within our channel we basically recognize three strong scattering objects. The received power through those objects is $10-15\,\mathrm{dB}$ weaker than for the LOS connection. The impinging field can be considered as directionally sparse. The receiving "hot spots" appear widespread due to convolution with the horn antenna pattern, which is spatially low pass filtering.

For the co-polarised scenario, the K-factor varies significantly between the LOS connection and the connection through scattering objects. In the cross-polarised scenario, the K-factor variation is reduced.

The RMS delay spread for the co-polarised case is very low for reflected signals. The desk is not reflective in the cross-polarised case and hence the RMS delay spread is very large there.

5 CONCLUSION

Measurements indicate that millimetre wave channels are less reverberant than their decimetre and centimetre wave counterparts [15]. Reliable reception is possible through specular reflections, where Rician fading distributions ($K \gg 0$) are seen.

Depending on the polarisation, interaction of objects is very different and beamforming algorithms should therefore also incorporate polarization information. Further, links should not only be established at scattering objects which enable high receive power; one has to take the RMS delay spread into account as well.

Acknowledgments

This work has been funded by the Christian Doppler Laboratory for Dependable Wireless Connectivity for the Society in Motion and the Institute of Telecommunications, TU Wien. The financial support by the Austrian Federal Ministry of Science, Research and Economy and the National Foundation for Research, Technology and Development is gratefully acknowledged.

References

[1] E. Zöchmann, S. Schwarz, and M. Rupp, "Comparing antenna selection and hybrid precoding for millimeter wave wireless communications," in *IEEE 9th Sensor Array and Multichannel Signal Processing Workshop (SAM)*, 2016.

[2] T. S. Rappaport *et al.*, "Millimeter wave mobile communications for 5G cellular: It will work!" *IEEE Access*, vol. 1, pp. 335–349, 2013.

[3] ——, "Broadband millimeter-wave propagation measurements and models using adaptive-beam antennas for outdoor urban cellular communications," *IEEE Transactions on Antennas and Propagation*, vol. 61, no. 4, pp. 1850–1859, April 2013.

[4] H. Xu, V. Kukshya, and T. S. Rappaport, "Spatial and temporal characteristics of 60-GHz indoor channels," *IEEE Journal on Selected Areas in Communications*, vol. 20, no. 3, pp. 620–630, Apr 2002.

[5] S. Geng *et al.*, "Millimeter-wave propagation channel characterization for short-range wireless communications," *IEEE Transactions on Vehicular Technology*, vol. 58, no. 1, pp. 3–13, Jan 2009.

[6] D. Dupleich *et al.*, "Double-directional and dual-polarimetric indoor measurements at 70 GHz," in *International Symposium onPersonal, Indoor, and Mobile Radio Communications (PIMRC)*, 2015.

[7] A. Maltsev *et al.*, "Impact of polarization characteristics on 60-GHz indoor radio communication systems," *IEEE Antennas and Wireless Propagation Letters*, vol. 9, pp. 413–416, 2010.

[8] E. Zöchmann *et al.*, "Resolving the angular profile of 60 GHz wireless channels by delay-Doppler measurements," in *IEEE 9th Sensor Array and Multichannel Signal Processing Workshop (SAM)*, 2016.

[9] B. H. Fleury, "First- and second-order characterization of direction dispersion and space selectivity in the radio channel," *IEEE Transactions on Information Theory*, vol. 46, no. 6, pp. 2027–2044, Sep 2000.

[10] F. van der Wijk, A. Kegel, and R. Prasad, "Assessment of a pico-cellular system using propagation measurements at 1.9 GHz for indoor wireless communications," *IEEE Transactions on Vehicular Technology*, vol. 44, no. 1, pp. 155–162, Feb 1995.

[11] K. Witrisal, Y.-H. Kim, and R. Prasad, "A new method to measure parameters of frequency-selective radio channels using power measurements," *IEEE Transactions on Communications*, vol. 49, no. 10, pp. 1788–1800, Oct 2001.

[12] P. Zetterberg and R. Fardi, "Open source SDR frontend and measurements for 60-GHz wireless experimentation," *IEEE Access*, vol. 3, pp. 445–456, 2015.

[13] K. Witrisal and A. Bohdanowicz, "Influence of noise on a novel RMS delay spread estimation method," in *International Symposium on Personal, Indoor and Mobile Radio Communications (PIMRC)*, 2000.

[14] P. L. C. Cheong, "Multipath component estimation for indoor radio channels," in *In Proceedings of Global Telecommunications Conference (GLOBECOM)*, 1996.

[15] A. F. Molisch *et al.*, "A comprehensive standardized model for ultrawideband propagation channels," *IEEE Transactions on Antennas and Propagation*, vol. 54, no. 11, pp. 3151–3166, Nov 2006.